Progress in Oceanography 188 (2020) 102447

Contents lists available at ScienceDirect

Progress in Oceanography

journal homepage: www.elsevier.com/locate/pocean

Productive detours – Atlantic water inflow and acoustic backscatter in the major troughs along the Svalbard shelf

Sebastian Menze [a,*], Randi B. Ingvaldsen [a], Anna Nikolopoulos [a], Tore Hattermann [b,c], Jon Albretsen [a], Harald Gjøsæter [a]

[a] Institute of Marine Research, P.O.Box 1870 Nordnes, 5817 Bergen, Norway
[b] Norwegian Polar Institute, Tromsø, Norway
[c] Energy and Climate Group, Department of Physics and Technology, The Arctic University – University of Tromsø, Norway

A B S T R A C T

Atlantic Water (AW) flowing along the western and northern Svalbard shelf-break extends the Atlantic domain into the Arctic and is the region's major source of heat, nutrients and advected plankton. We investigated the inflow and recirculation of AW into four major troughs that cut into the Svalbard shelf, the Isfjorden, Kongsfjorden, Hinlopen and Kvitøya Troughs, and related the circulation patterns to acoustic backscatter observed with echosounders and Acoustic Doppler Current Profilers. The acoustic observations showed higher levels of backscatter from fish in the Hinlopen Trough compared to the shelf and shelf-break north of Svalbard. This coincides with a steady inflow of nutrients, biomass and heat into the trough with the AW. Trough circulation was characterized using output from a high-resolution regional ocean model and particle tracking simulations. All four troughs experience topographically steered recirculation (in-and-outflow) of AW, but the troughs on the western Svalbard shelf showed a stronger seasonality than the troughs on the northern shelf. The Hinlopen Trough receives the strongest AW inflow and the most direct inflow from the shelf-break boundary current. The troughs form hybrid habitats between the shelf and shelf-break that extend the Atlantic advective domain closer to the Svalbard coastline.

1. Introduction

The Svalbard shelf forms a transition zone between boreal, arctic and coastal ecosystems, whose boundaries are changing with global warming (Fossheim et al., 2015; Haug et al., 2017). The shelf rises from approx. 2500 m to 200 m depth, and is characterized by multiple cross-shelf troughs and fjord systems that were formed by ice streams during past glacials (Vanneste et al., 2010). Four trough systems are deeper than 200 m (Fig. 1): the Isfjorden Trough (IT), the Kongsfjorden Trough (KT), the Hinlopen Trough (HT) and the Kvitøya Trough (KviT). Whereas the IT, KT and KviT mouth fans are smooth continuations of the Svalbard shelf slope, the opening of HT faces a steep drop named Malenebukta that was created by a marine megaslide 30 000 years ago (Geissler et al., 2016; Vanneste et al., 2006; Winkelmann et al., 2008).

Roughly half (~1.8 Sv) of the Atlantic Water (AW) flowing northward from the Nordic Seas enters the Barents Sea (Skagseth et al., 2008) where it loses much of its heat and is significantly transformed before entering the Arctic (Smedsrud et al., 2013). In contrast, the AW flowing around Svalbard (~2 Sv) retains its upstream properties longer and is known to create an ice-free area along the Svalbard shelf termed "Whalers Bay" (Beszczynska-Moller et al., 2012; Koenig et al., 2017; Pérez-Hernández et al., 2019). The warm and saline AW flows along the Svalbard shelf as a boundary current, termed the West Spitsbergen Current (WSC) and Arctic Circumpolar Boundary Current north-east of Svalbard. This current is the major heat, carbon and plankton supply to the Arctic Ocean and is an important feature of the earth's climate system (Wassmann et al., 2015; Bluhm et al., 2015). AW is also known to spread onto the Svalbard shelf and into the troughs. This has been best studied in Isfjorden and Kongsfjorden (Nilsen et al., 2016). The inflow to the shelf and troughs are controlled by multiple forces: the WSC volume transport and hydrographic structure, the wind and sea surface height field, internal waves, topographic steering and eddy overturning (Cottier et al., 2005, 2007; Inall et al., 2015; Nilsen et al., 2016; Tverberg & Nost, 2009). In this paper we investigate how topographically steered currents transport AW into the four major troughs and discuss how this renders the troughs special habitats along the shelf.

The AW flowing around Svalbard is warming in parallel with global trends and increasingly releases its heat to melt sea ice from below due to reduced stratification (Beszczynska-Moller et al., 2012; Polyakov et al., 2017; Lind, et al., 2018). The Barents and Svalbard region are experiencing some of the fastest warming on the planet (up to 0.08 °C/yr, Asbjørnsen et al., 2020) and the region's sea ice cover is rapidly

* Corresponding author at: Institute of Marine Research, Bergen, Norway.
E-mail address: sebastian.menze@hi.no (S. Menze).

https://doi.org/10.1016/j.pocean.2020.102447

Available online 30 September 2020
0079-6611/© 2020 The Author(s). Published by Elsevier Ltd. This is an open access article under the CC BY license (http://creativecommons.org/licenses/by/4.0/).

retreating (up to 3%/yr, Asbjørnsen et al., 2020). The loss of sea ice and increasing "Atlantification" of the area impacts Arctic and ice-dependent species and opens new habitat for boreal species and human activity (Haug et al., 2017). Svalbard has historically been a hunting ground for marine mammals. Bowhead whales and walrus that were hunted to near extinction between 1600 and 1900, which likely benefited seabirds and fish (Węsławski et al., 2000). With the Atlantification of the ecosystem, advent of modern trawling vessels and receding sea ice, active fisheries have developed on the Svalbard shelf (Misund et al., 2016). They focus mainly on the demersal Northeast Arctic cod (*Gadus morhua*) and Northeast Arctic haddock (*Melanogrammus aeglefinus*) as well as Northern shrimp (*Pandalus borealis*). Maps of cumulative fishing activity in the Svalbard area show highest fishing intensity in Hinlopen Strait, trawling for Northern shrimp, followed by Isfjorden, Bellsund outside of Van Mijenfjorden and Kongsfjorden, and moderate and less localized fishing activity along the western shelf slope (Misund et al., 2016). Surveys of benthic biomass north of Svalbard found rich benthic communities in the Hinlopen Strait, and suggested that this was caused by a large supply of organic matter from inflowing AW, as benthos growth in the area is primarily food limited (Carroll and Ambrose, 2012; Meyer et al., 2015). Baleen whales are frequently observed in Hinlopen Strait and on the shelf-break north of Svalbard (Storrie et al., 2018; Vacquié-Garcia et al., 2017). Habitat suitability modelling indicates that some troughs are favorable habitats for fin, blue and humpback whales (Storrie et al., 2018). Ressler et al. (2015) showed a correlation between fin and humpback whale sightings and euphausiids backscatter for the Barents Sea and Svalbard area, with some of the highest euphausiid backscatter values in Hinlopen Strait. In this study, we are investigating how the inflow of nutrient- and biomass-rich AW could render some troughs favorable habitats along the shelf.

2. Methods

In this study we analyze hydrographic and acoustic backscatter data measured during multiple scientific surveys and current velocities modelled with a hydrodynamical model.

2.1. ADCP and echosounder data

We used data from both Simrad EK60 Echosounders and 75 kHz RDI Acoustic Doppler Current Profilers (ADCPs) to analyze patterns in acoustic backscatter along the Svalbard shelf. The vessel mounted ADCP dataset is described in Menze et al. (2019) and covers the July, August and September months 2014 to 2017. In addition, ADCP data from cruises conducted with *RV Helmer Hanssen* between the 14th September and 2nd October 2018 and 19th September and 4th October 2019 are used. We calculated the Nautical area scattering coefficient s_A (m^2 nmi^{-2} MacLennan et al. (2002)) from the ADCP Received Signal Strength Indicator (RSSI) following a standard method developed by Deines (1999), arriving at levels that compare well to an analysis of ADCP backscatter in the area by Berge et al. (2014). ADCP signals are mainly scattered by zooplankton and other particulate matter in the mm to cm range (Fielding et al., 2004; Gostiaux and van Haren, 2010). The ADCPs were not calibrated with tungsten-carbide spheres and thus the ADCP backscatter values only contain relative information, so that it is possible to compare the patterns between the echosounder and ADCP, but not absolute values.

Echosounder data were collected during 6 surveys with *RV Helmer Hanssen* in August and September 2014 to 2019, with a Simrad EK60 echosounder at 18 kHz, 38 kHz and 120 kHz at 1 ms pulse duration. The surveys and echosounder data are described in detail in Ingvaldsen et al. (2016a, 2016b, 2017a, 2017b) and Meeren and Prozorkevich (2019) and first analyses of a part of the echosounder data have been conducted in Gjøsæter et al. (2017), Knutsen et al. (2017) and Ingvaldsen et al. (2017a). The echosounders were connected to transducers mounted on a protruding instrument keel with transducer faces ~ 3 m below the hull; normally ~ 8.5 m below the sea surface. Multi-frequency scrutinization and target strength analysis were conducted with the Large Scale Survey

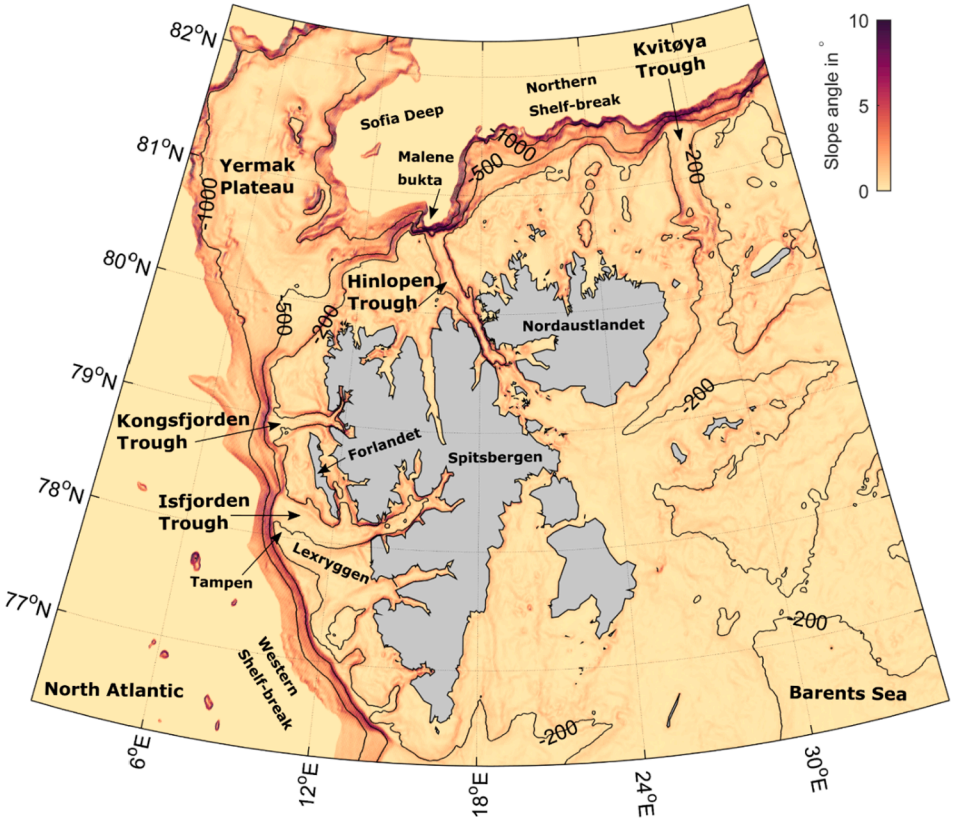

Fig. 1. Map of the study area and major topographic features. The black contours mark the 1000, 500 and 200 m isobath, the yellow–red colors show the slope angle. The depth was truncated at 1500 m and the angle colormap at 10°. The slope angle in front of the Hinlopen trough was approx. 20°. The bathymetric data was retrieved from the International Bathymetric Chart of the Arctic Ocean (Jakobsson et al., 2012). (For interpretation of the references to color in this figure legend, the reader is referred to the web version of this article.)

System (LSSS) post-processing system (Korneliussen et al., 2006, 2016) which also was used for exporting files for subsequent analysis. The scrutinized processing involved spike-filtering (to remove unwanted acoustic temporal noise from e.g. trawl sensors during trawl operations), compensation for the placement of transducers, and noise removal. The interpretations were made per standard procedures where the total backscatter was split into target categories (Korneliussen et al., 2016). Details of the interpretation can be found in Knutsen et al. (2017) and Gjøsæter et al. (2017). For this study the target categories were collected into drifting organisms (plankton, young-of-the-year fishes and mesopelagic fishes) and fish (all larger fishes not drifting with the ocean currents). The scrutinized acoustic backscattering data in the echosounder output were in the form of s_A, Nautical area scattering coefficient in standard units; (m^2 nmi^{-2} MacLennan et al. (2002)). They were integrated to 10 m depth bins from below the hull mounted 38 kHz transducer to below 700 m.

2.2. Hydrographic and sea ice data

Vertical profiles of temperature and salinity were measured with a Sea-Bird Scientific SBE911plus Conductivity-Temperature-Depth profiler (CTD) during surveys with *RV Helmer Hanssen*. The locations and dates of the CTD profiles are given in Suppl. Table 1. For the hydrographic data, we define AW as water warmer than 0 °C and more saline than 34.9 PSU, (Rudels et al., 2005).

Sea ice concentration data was obtained from the University of Bremen, based on the Advanced Microwave Scanning Radiometer Earth Observing System (Spreen et al. 2008). The trough outlines were defined by the 200 m isobath using the International Bathymetric Chart of the Arctic Ocean (IBCAO) bathymetry dataset (Jakobsson et al., 2012).

2.3. Hydrodynamical model

For exploring the ocean circulation and hydrography of the study area in a fuller, three-dimensional view we complemented our analysis with data of daily averaged current velocity, temperature and salinity from the S800 high-resolution (800 m × 800 m grid size) simulation using the Regional Ocean Modeling System (ROMS, http://myroms.org, see e.g. Budgell, 2005; Haidvogel et al., 2008; Shchepetkin and McWilliams, 2005) covering the Svalbard area. Details on the S800 model set up can be found in the earlier publications of Hattermann et al. (2016), Crews et al. (2018) and Crews et al. (2019). The ROMS simulations were validated against data from ADCPs moored in Fram Strait and surface current observations from drifters in Hattermann et al. (2016) and against salinity and temperature time-series from the northeast of Svalbard in Crews et al. (2018).

The S800 model was run for the years 2007 to 2010, which is before the 2014 to 2019-time period during which the backscatter and CTD observations were taken. Thus, we could not compare the temporal variability between the model and backscatter dataset, only averaged spatial patterns. We accepted this offset in time since updated high-resolution simulations synchronous with the observational period are not yet available, and because we are focusing on spatial patterns associated with topographic steering of the AW flow (which do not change over time) rather than a temporal analysis. We extracted model results for sections across the troughs to calculate the AW inflow, using the component of the modelled flow that was oriented normal to the transects. For the model sections we define AW as water warmer than 0 °C and more saline than 34.8 PSU to include AW modified by cooling and mixing along its pathway and to avoid a slight bias of the model towards lower salinity in the entire domain (Crews et al., 2019).

To study the pathways of seawater and drifting organisms into the troughs, we calculated particle trajectories through the S800 daily averaged model fields using TRACMASS (Döös, 1995). We used the same S800 model fields (for all years 2007–2010) and tracking algorithm as described in Hattermann et al. (2016) and Silyakova et al. (2020). Particles were seeded across the entire water column in 5-day intervals (during the entire model period) along 4 transects across the shelf-break, located upstream of each of the 4 troughs. The particles were given a lifetime of 60 days.

3. Results

3.1. Hydrodynamics of the four trough systems

Fig. 2 shows summer-time temperature and salinity sections along IT, KT and HT, as measured in September 2014. Outside IT, AW is centered at the shelf-break (the salinity maximum indicates the WSC core) and stretches into the trough and fjord. Within the IT, AW occupies the water column from the sea floor to the upper tens of meters, where a fresher and warmer layer of Polar Surface Water (PSW) lies atop the AW. KT shows a similar hydrography but a less fresh PSW layer. In HT, AW is colder, and is visible as a high salinity core on the shelf-break outside the trough, and extends all the way into the trough (that is slightly fresher than in IT and KT). The PSW layer is considerably fresher and colder in HT than in IT and KT.

KviT and HT contain considerably more sea ice than IT and KT on the western Svalbard shelf. During the years of the ADCP and echosounder observations (2014–2019) the average number of annual sea ice days (sea ice concentration > 15%) were 1 for the IT and KT, 83 for the HT and 230 for the KviT, derived from Advanced Microwave Scanning Radiometer Earth Observing System II sea ice concentration data using the 200 m isobath as trough border.

3.1.1. Hydrodynamical model

The horizontal circulation patterns in the four trough systems were calculated as depth and time averages over all S800-model years (2007–2010) and are shown in Figs. 3 and 4. Monthly averages of the circulation patterns in the troughs are presented in suppl. Fig. 1–4 and maps of monthly averaged salinity and temperature are shown in suppl. Fig. 5 and 6.

The WSC is visible as a strong northward boundary current along the shelf slope between the 300 and 1000 m isobaths (Fig. 3). The offshore and shelf slope branches of the WSC merge near the opening of the IT (Fig. 3b).

The circulation system of the IT is dominated by topographic steering and three major inflows are discernible in the average current map (Fig. 3b). An AW inflow branch (marked with a blue 2) follows the 200 m isobath onto the shelf and then merges with the Svalbard coastal current (roughly following the 100 m isobath, marked with a blue 1) to jointly follow the southern trough slope to the entrance of Isfjorden. This current branch then recirculates as a narrow and strong outflow current along the northern trough slope. Another AW inflow branch enters at the northern opening of the IT, but this one merges with the strong outflow current instead of flowing further into the trough (marked with a blue 3).

In KT, a single AW inflow branch is circulating in the trough system roughly following the 200 m isobath (Fig. 3a). Its origins are in the WSC and the Spitsbergen Trough Current that transport AW out of the IT parallel to the WSC. The topographically steered current flowing out of KT partly coalesces with the WSC again.

The shelf-break north of HT is characterized by steep slopes and canyons, creating a V-shaped feature named Malenebukta, that faces the steep shelf-break in front of the trough opening. The average AW boundary current follows the large-scale bathymetry of the shelf-break and is only marginally deflected by the irregular slope bathymetry (Fig. 4). Two inflows into HT are discernible: an AW branch entering the trough on the western side of the opening and roughly following the 200 m isobath (blue 1 in Fig. 4a), and a coastal current branch following the 100 m isobath along the coast into Hinlopen strait (blue 2 in Fig. 4a). A large part of the inflowing AW branch flows southward into the trough, but part of the inflowing AW is deflected and recirculated on the shelf

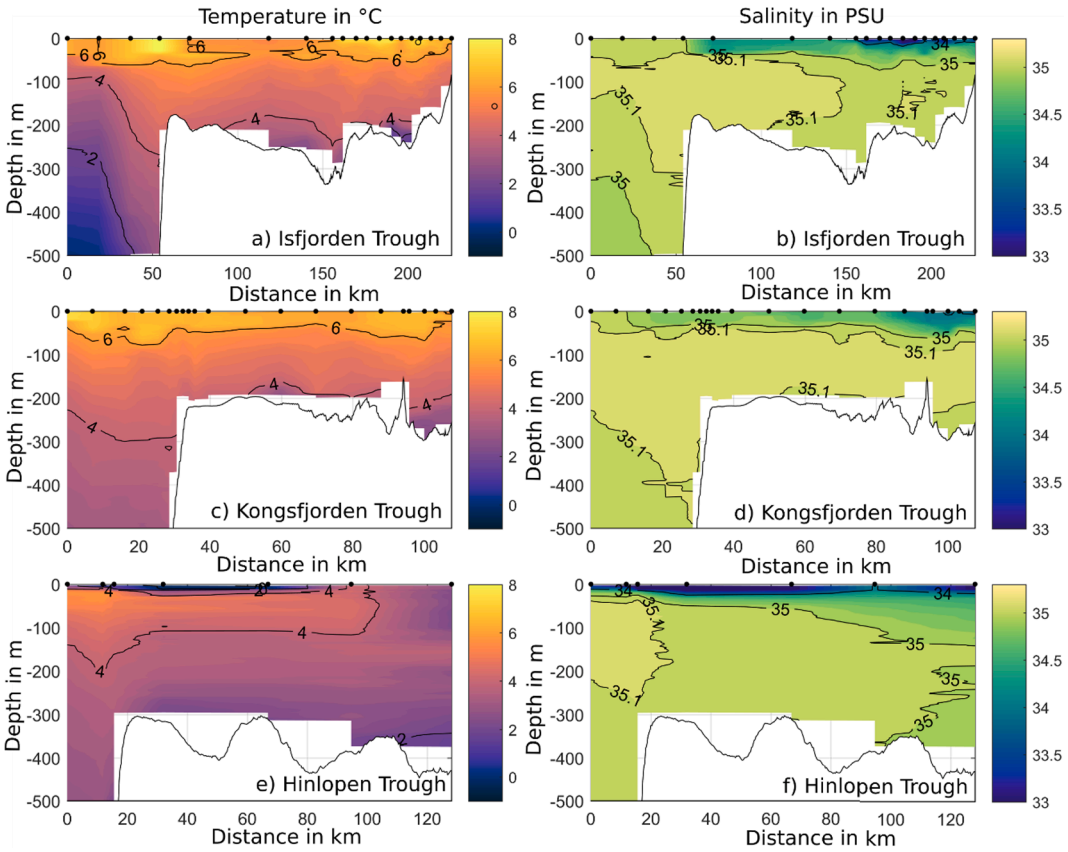

Fig. 2. CTD temperature and salinity sections along the four troughs measured during August and September 2014 for the Isfjorden, Kongsfjorden and Hinlopen troughs (panel a-f). Black dots indicate locations of CTD stations. White outline shows the IBCAO based bathymetry along the section. The shelf-break is located to the left in the panels.

west of the HT. There it merges with the coastal current branch and flows southward into the trough as slope current. The slope current turns northward at ~ 79°33′ N and exits the trough following the eastern slope of the trough. Parts of the outflow merges back with the WSC and parts of it diverts over the shelf east of HT.

The circulation in the KviT (Fig. 4b) is characterized by a strong southward flowing current on the western trough slope comprising inflow from the eastern shelf (blue 2 in Fig. 4b), inflow of AW from the boundary current (blue 1 in Fig. 4b), and a recirculating flow inside the trough. The topography of KviT features a 300 m deep rise at the opening of the up to 400 m deep KviT. At this rise eastward flowing AW faces westward flowing shelf water. Most of the southward flowing water in KviT follows the 200 m isobath into the northern Barents Sea, but smaller amounts also recirculate in the trough.

To give an overview of the seasonal cycle of inflow and hydrography we averaged modelled current velocity, temperature and salinity sections across the four troughs over the months of September, December, March and June 2007–2010. Fig. 5 shows the seasonality of Section 2 in HT, Suppl. Fig. 7 shows the seasonality of the IT Section 2, Suppl. Fig. 8 the KT section and Suppl. Fig. 9 the KviT section. The topographically steered recirculation patterns dominate the velocity sections of all the 4 troughs in all months.

In IT (Suppl. Fig. 7) the inflow is strongest in December and March, and outflow strongest in September. Temperatures are highest in September, and AW in the trough is discernible through high temperature and salinity values. In December and March, the AW inflow is visible as a core of raised temperature and salinity, in June mainly in salinity. In June and September, the upper tens of meters of the sections are covered by a warm PSW layer that erodes with convection in the fall and winter.

The KT (Suppl. Fig. 8) shows a seasonality similar to IT. AW inflow and outflow are present in all four months and strongest in December and March while weaker in June. A PSW layer is present from spring to fall, and AW inflow is visible as increased temperature and salinity values on the southern trough slope.

The inflow current into HT (Fig. 5) shows less seasonal variation than for IT and KT. The outflow current shows an additional gravity current of cold and haline water flowing northward in December and March. Both the AW in- and outflows are visible in the temperature section in September, December and June, while in March only the temperature signature of the inflow is visible. The temperature sections show a clear seasonal cycle. The inflow is also discernible as increased salinity on the western trough slope. In June and September, the upper tens of meters are covered by a warm PSW layer. The gravity current indicated in the temperature and salinity sections for December and March likely transports brine enriched winter water formed by sea ice formation on the shelf or in the trough.

Similar to the HT, the inflow current into KviT (Suppl. Fig. 9) shows limited seasonal variation, but the outflow in winter is characterized by a northward flowing gravity current of cold and brine enriched winter water. The inflow is visible as a temperature maximum and faintly as a salinity maximum, indicating a combination of both AW and shelf water as source of the inflow. The temperature sections show a clear seasonal cycle. This section is overall colder and fresher than the previous three locations and characterized by cold and fresh shelf water on the eastern side of the trough and brine enriched winter water in the deepest parts of the trough.

We compared the inflow into the four trough systems using transport time series through six sections (Fig. 6 and Table 1). The average inflow was highest in KviT, although most of the inflow there was derived from the shelf instead of the AW boundary current, followed by the HT, IT and KT. When calculating only the transport of AW and modified AW

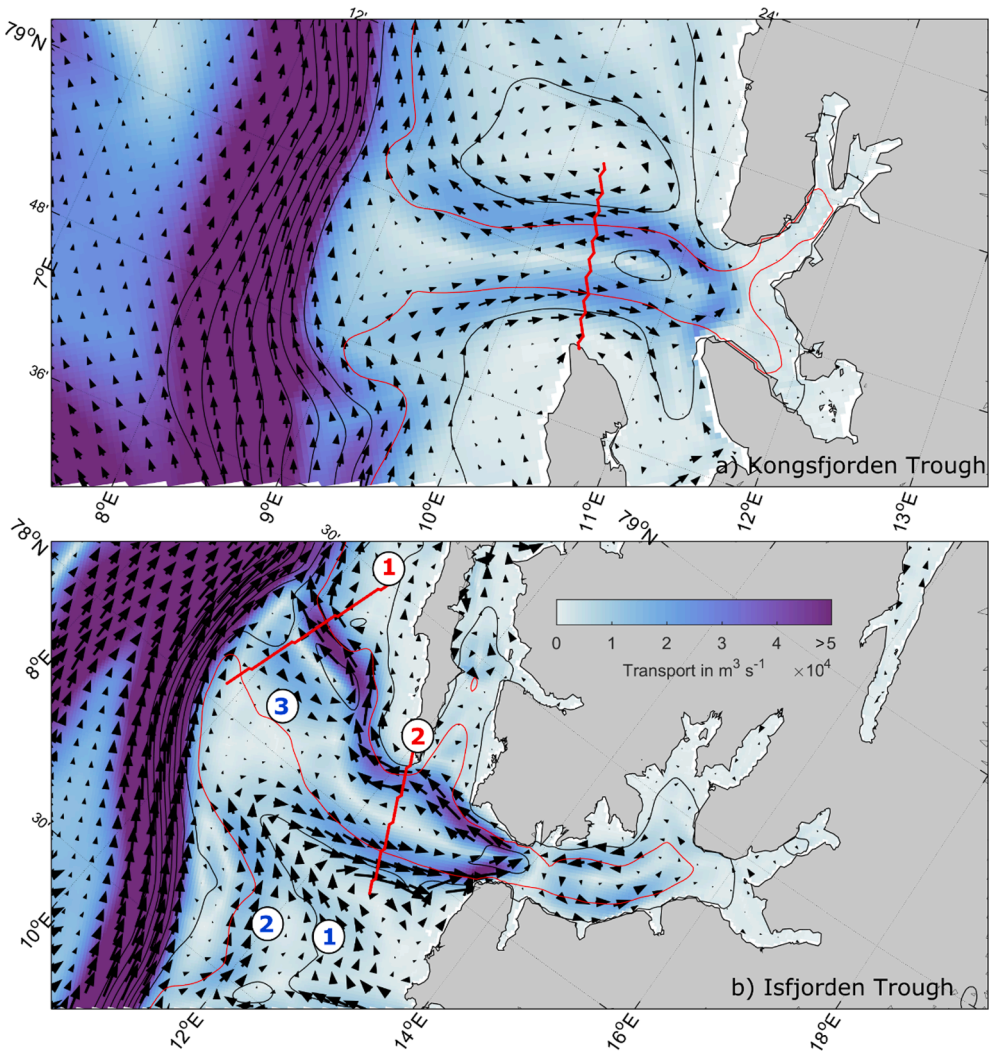

Fig. 3. Maps of depth and time averaged circulation patterns in the Isfjorden and Kongsfjorden troughs. Black contours indicate model bathymetry in 100 m intervals, while red contour indicates the 200 m isobath. Color shades indicate the horizontal transport integrated over the upper 600 m, capped at $5x10^4$ m^3 s^{-1}. Black arrows are plotted only at a subset of model grid cells for better visualization. Thick red lines and numbers crossing the troughs mark the sections used to calculate inflow. Blue numbers mark the inflow currents. (For interpretation of the references to color in this figure legend, the reader is referred to the web version of this article.)

(temperature > 0 °C and salinity > 34.8 PSU), HT had the highest average inflow followed by IT, KviT and KT.

The total and AW transport time series (Fig. 6) for the troughs west of Svalbard (IT and KT) show a clearer seasonal cycle with stronger inflow in winter than summer than the troughs north of Svalbard (HT and KviT). North of Svalbard a seasonal cycle is mainly visible in the AW transport.

The first principal component (1. PC) of the velocity sections of all troughs was the recirculation (in- and out-flow) pattern. Suppl. Fig. 10 shows the Empirical Orthogonal functions (EOFs) of the 1. PC for the six sections. The amount of variation explained by the 1. PC was highest for the HT with 66%, followed by 50% for the KT, 48% for the IT and 46% for the KviT. The time series of the 1. PCs are shown as blue lines in Fig. 6 and match the black transport time series well. The 1. PC shows higher values (higher presence) in summer than winter for both the IT and KT, and less seasonal variation for the HT and KviT. In the HT and KviT the total transport and 1. PC timeseries agree well with each other and exhibit less seasonal variation than the AW transport time series. This indicates that the seasonality of AW inflow north of Svalbard is mainly caused by variation in AW properties, i.e. increased cooling of the AW in winter, rather than volume transport.

3.1.1.1. Particle tracking. We analyzed the trajectories of particles that were released across the shelf-break to study the connectivity between the shelf-break and the troughs and determine the origins of the trough water. Fig. 7 shows the pathways of particles seeded along a cross-shelf transect (marked with red lines) and making it into the troughs. Only trajectories that cross the 200 m isobath (based on the IBCAO bathymetry) into each trough and are at least a day inside the trough are shown. The origins of the particles that enter the troughs are shown on the seeding transects in Fig. 8, with the colored sections indicating the percentage of released particles per grid cell that enter the trough.

For IT, most of the inflowing particles come from the shelf, following the boundary current around Lexryggen. This pathway is visible as a yellow track in Fig. 7a. A smaller number of particles also derives directly from the WSC (along the shelf-break) and enters the trough opening around Tampen (Toponym shown on map in Fig. 1). KT receives particles mainly from the shelf and very few directly from the shelf-break (yellow areas in Fig. 7b and Fig. 8b).

The particles entering HT and KviT derive directly from the AW boundary current along the shelf-break (Fig. 8). Of all the troughs, HT received the most particles from the AW boundary current. Most particles entering HT follow the topographically steered inflow of AW into the trough (yellow area in Fig. 7c). In addition, particles from the shelf enter the trough with the Svalbard coastal current (Fig. 7c). KviT also receives particles from the AW boundary current, but they do not flow as far into KviT as they do in HT (Fig. 7d and Fig. 8d).

3.2. Acoustic backscatter

To compare acoustic backscatter in different regions, we averaged backscatter profiles on the shelf, shelf-break, and in IT, KT and HT using

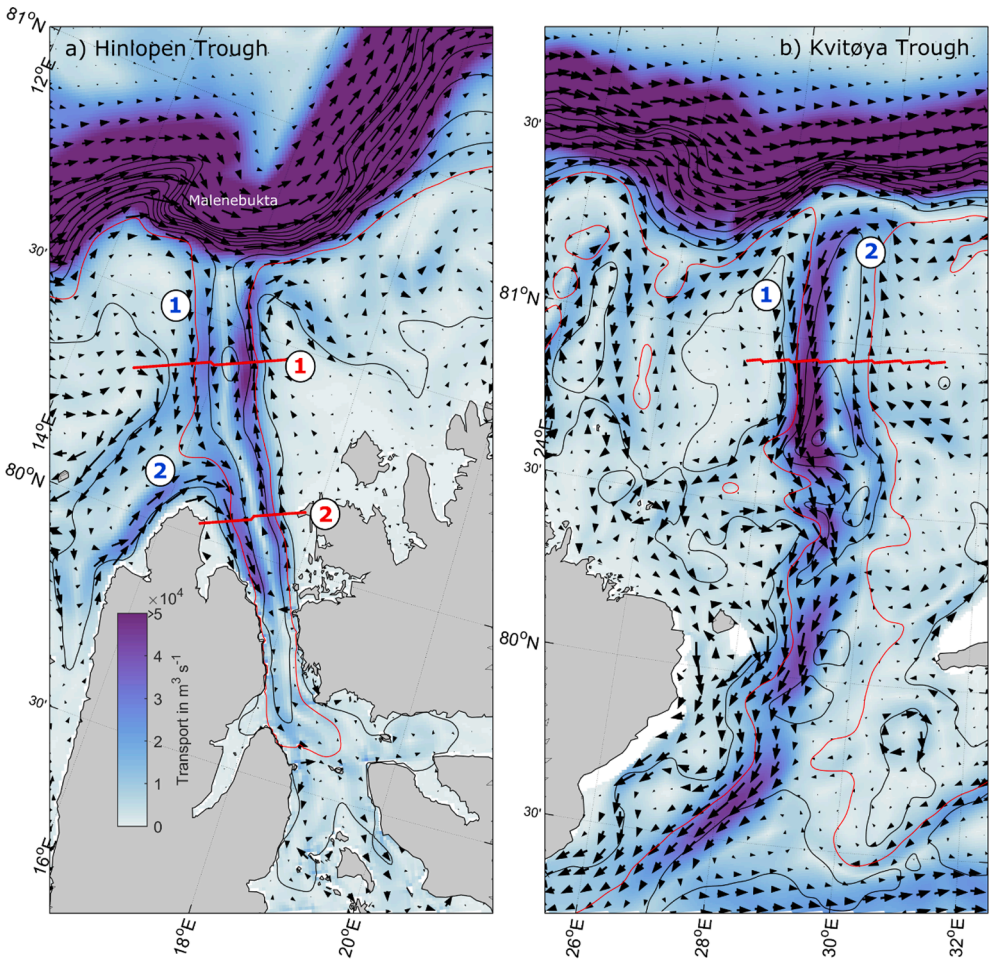

Fig. 4. Maps of depth and temporally averaged circulation patterns in the Hinlopen and Kvitøya trough. Black contours indicate model bathymetry in 100 m intervals, red contour indicates 200 m depth. Color hues indicate transport in the upper 600 m through model bins, capped at $5x10^4$ m^3 s^{-1}. Black arrows are plotted only at a subset of model bins for better visual distinction. Thick red lines and numbers crossing the troughs mark the sections used to calculate inflow. Blue numbers mark the inflow currents. (For interpretation of the references to color in this figure legend, the reader is referred to the web version of this article.)

38 kHz echosounder and 75 kHz ADCP data. A map of the echosounder profile locations is shown in Fig. 9 and the averaged profiles are shown in Fig. 10. The ADCP profile locations were almost identical to the echosounder profile locations and are shown in Suppl Fig. 11. Echosounder and ADCP data were only sufficiently sampled on the shelf and shelf-break north of Svalbard and in HT. The profiles in Fig. 10 were averaged using data from all available years (2014–2019). Comparisons of averaged backscatter profiles for each year are presented in Suppl. Fig 12–14. For the shelf-break we averaged profiles with bottom depths between 200 and 1000 m. For the shelf we averaged profiles with bottom depths between 50 and 200 m and for HT we averaged profiles between 200 and 400 m bottom depth inside the 200 m isobath outlining HT.

On the shelf-break (yellow profiles), the 38 kHz backscatter from drifting organisms was strongest in the surface layer (0–100 m depth), followed by a smaller increase in the mesopelagic layer between 300 and 500 m (Fig. 10a), whereas the 38 kHz backscatter from fish on the shelf-break was strongest in the mesopelagic layer (Fig. 10b). The ADCP backscatter on the shelf-break was strongest in the surface layer, followed by a sharp decrease at ~ 50 m depth and a gradual increase to around ~ 400 m depth (Fig. 10c). Suppl. Figure 12–14 confirm that these patterns were present each year.

On the shelf (red profiles), the 38 kHz backscatter from drifting organisms showed a peak in the surface layer whereas the 38 kHz backscatter from fish increased towards the bottom. The ADCP backscatter on the shelf was strongest towards the bottom, showing levels similar to the deeper layer in HT (Fig. 10c). The surface layer ADCP backscatter was almost equal on the shelf and shelf-break.

In HT, the 38 kHz backscatter from drifting organisms showed a peak in the surface and mesopelagic layer (blue profile, Fig. 10a). Towards the bottom, 38 kHz backscatter from drifting organisms was stronger in HT than on the shelf-break. Of all the sampled areas, 38 kHz backscatter from fish was strongest in HT, with levels increasing towards the bottom (Fig. 10b). Average ADCP backscatter in the surface layer was strongest in HT compared to the other sampled areas (Fig. 10c), this was the case during the surveys in 2016, 2017 and 2018 whereas in 2019 surface layer ADCP backscatter was lower in HT than on the shelf break (Suppl. Fig. 14).

Fig. 11 compares the averaged vertical distribution of temperature, salinity and fluorescence with backscatter profiles in HT. The backscatter peaks in the surface layer (in the euphotic zone) are located in a strongly stratified warm Polar Surface Water layer. The surface layer backscatter peaks were recorded in depth just below the peak in fluorescence, near the base of the halocline. This indicates that the high acoustic backscatter levels are related to local production in the Polar Surface Water layer, possibly fueled by upward mixing of nutrients from the nutrient-rich AW. The high backscatter from fish in the lower layers was located in the modified AW with temperatures above 2 °C.

4. Discussion

We found that AW flows into all four troughs, with HT receiving the largest AW inflow of the four troughs. Whereas the total trough inflow on the western Svalbard shelf showed a marked seasonal cycle and increase in winter, the total trough inflow on the northern shelf showed less seasonality. The particle tracking simulations showed that inflow into the western Svalbard troughs derives from both the shelf-break and shelf, whereas inflow into HT derives directly from the shelf-break. HT

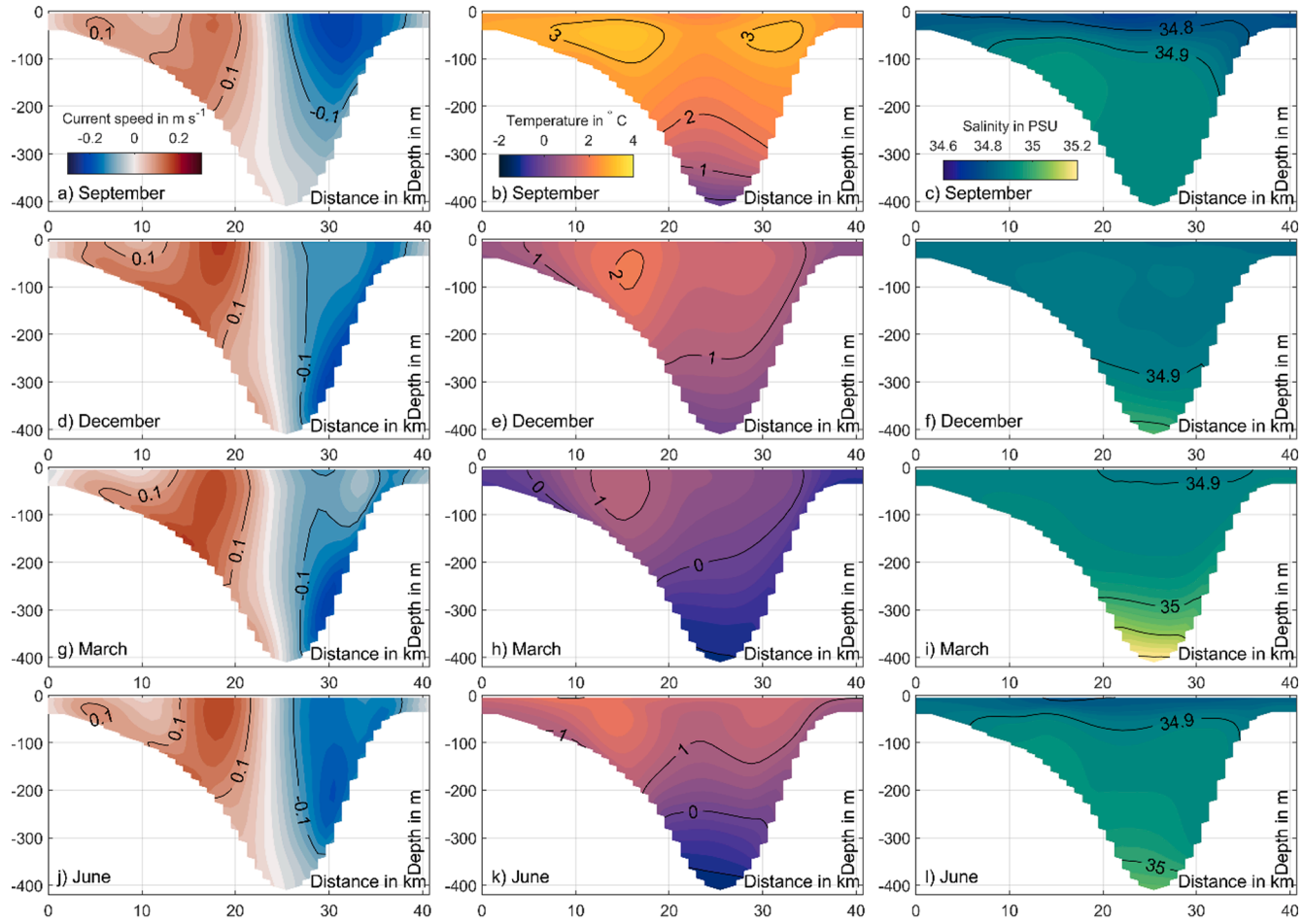

Fig. 5. Seasonal cycle for the Hinlopen trough Section 2 (marked with red line in Fig. 2) of in- (red) and outflow (blue, left panels) temperature (middle panels), salinity (right panels) and for September, December, March and June from the S800 model. The data are averaged over the 4 model years (2007–2010). Color hues range −0.3 to 0.3 m s^{-1} for the currents, −2 to 4° for temperature and 34.6 to 35.2 PSU for salinity. The left side of the section faces west and the right side east. (For interpretation of the references to color in this figure legend, the reader is referred to the web version of this article.)

also showed stronger backscatter from fish in the trough than on the surrounding shelf and shelf break.

When interpreting the observed and modelled hydrography and backscatter distribution patterns, it should be kept in mind that the time period for model (2007–2010) and observations (2014–2019) did not overlap. Thus, temporal variability in the two datasets cannot be directly linked. Nevertheless, due to the strong topographic steering of the flow, the averaged S800 model hydrography and circulation patterns prove to be useful to interpret the differences between backscatter on the shelf, shelf-break and in Hinlopen Trough and discuss the impact of AW inflow on the trough ecosystems.

AW is a major source of nutrients and advected plankton to the Arctic Ocean, Svalbard shelf and fjords (Wassmann et al., 2015; Basedow et al., 2018; Randelhoff et al., 2018). A modelling study by Vernet et al. (2019) on the effect of AW advection on primary production found that advection provides 5–50 times more phytoplankton biomass than local production in the AW boundary current. They found that advected phytoplankton initiates blooms north of Svalbard in August and September that fuel the local benthic and pelagic ecosystems. A similar modelling study by Wassmann et al. (2019) found that 12 times more zooplankton biomass was advected than locally produced along the shelf north of Svalbard and that advected plankton is a major food source for fish, birds, and whales. Our analysis of observations and model data suggests that a part of this advected plankton is transported into the major troughs along the Svalbard shelf, forming favorable feeding areas for fish, marine mammals and benthic organisms.

4.1. Trough circulation

AW inflow into the Svalbard fjord and trough systems has earlier been studied with surveys, moorings and models, focusing especially on the Isfjorden and Kongsfjorden systems. Multiple mechanisms control the flow of AW into the troughs and onto the shelf: topographic steering (Nilsen et al., 2016; Saloranta and Svendsen, 2001), wind, upwelling and sea surface height differences (Cottier et al., 2007; Goszczko et al., 2018), eddy overturning (Tverberg and Nost, 2009) and the density gradients between AW, shelf and fjord water (Nilsen et al., 2008; Tverberg & Nost, 2009).

The circulation patterns of the S800 model show persistent topographically steered in- and out-flow currents in all four troughs (Figs. 3 and 4, Suppl. Figs. 1–4). The in- and out-flow pathways into IT and KT agree well with modelling efforts by Nilsen et al. (2016). They termed the AW current that enters IT and KT the Spitsbergen Trough Current (STC), and showed that the WSC and shelf waters connects to Isfjorden via two pathways: a direct inflow into the trough located at the trough opening (marked with blue 3 in Fig. 3) and an inflow following the 100 m isobath over the shelf (along the undersea ridge termed Lexryggen, marked with blue 2 in Fig. 3). The particle tracking indicated that the branch that originates on the shelf (blue 2 in Fig. 3) dominates the inflow into IT (Figs. 7 and 8). Our transport calculation for inflow into the IT (0.30 Sv) is a magnitude larger than presented Nilsen et al. (2016). This can be related to the higher resolution of the S800 model compared to the shelf model by Nilsen et al. (2016) or to a potentially exaggerated

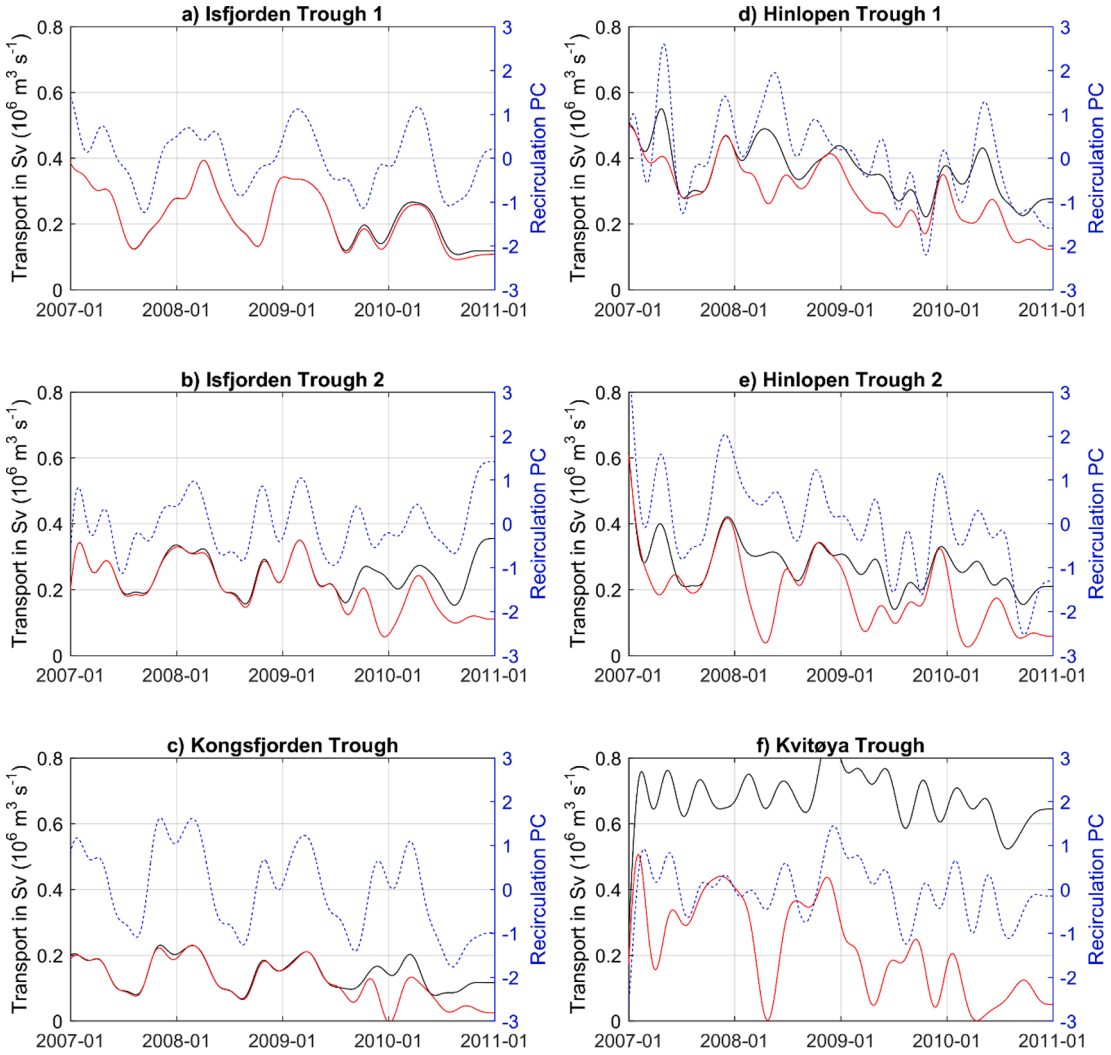

Fig. 6. Comparison of inflow time series for the four troughs (six transects). The black line represents low-pass filtered inflow, the red line low-pass filtered inflow of AW and modified AW (temperature > 0 °C and salinity > 34.8 PSU) and the blue dashed line the low-pass filtered strength of the 1. PC (the recirculation component of the velocity section). The low-pass filter was a 300 day 6th order Butterworth filter. (For interpretation of the references to color in this figure legend, the reader is referred to the web version of this article.)

Table 1
Comparison of inflow statistics for the four troughs based on sections extracted from S800 model data. The Empirical Orthogonal functions (EOFs) of the first Principal component (PC) are shown in Suppl. Fig. 4.

	Average inflow and standard deviation in Sv	Average AW inflow and standard deviation in Sv	Percentage of variation explained by 1st PC (Recirculation componen)
Isfjorden Trough 1	0.32 ± 0.21	0.30 ± 0.21	47
Isfjorden Trough 2	0.28 ± 0.12	0.23 ± 0.14	48
Kongsfjorden Trough	0.16 ± 0.06	0.13 ± 0.07	50
Hinlopen Trough 1	0.42 ± 0.15	0.33 ± 0.14	54
Hinlopen Trough 2	0.27 ± 0.13	0.19 ± 0.14	66
Kvitøya Trough	0.71 ± 0.19	0.25 ± 0.20	46

topographic steering in the S800 model. Like the Nilsen et al. (2016) model, the S800 model shows that the Isfjorden outflow partly rejoins the WSC and partly flows over the shelf alongside the WSC as the STC, which in turn recirculates in KT before merging with the Svalbard branch of the WSC to cross the Yermak Plateau (Fig. 3). The recirculating flow in KT is the shortest recirculation pattern of the four troughs, and also experiences the most pronounced seasonal cycle (Fig. 6). The particle tracking confirms that flow into KT originates from the shelf and STC (Figs. 7 and 8).

Previous modeling studies (Hattermann et al., 2016; Wekerle et al., 2017), ADCP observations (Menze et al., 2019) and the CTD sections from this study indicate that AW frequently recirculates within Hinlopen trough and strait. This result emerged also in the present analysis of the S800 model data. The HT receives the most AW inflow of the four troughs, probably facilitated by the bathymetry of the shelf-break and trough opening. The particle tracking showed that, of the four troughs, HT receives the most direct inflow from the AW boundary current (Fig. 8). The slope angle is far steeper off the HT than at any other locations along the shelf-break (Fig. 1). In the S800 model the slope angle at the shelf-break off HT's opening is ~ 10° due to the models coarse resolution. This is considerably lower than both IBCAO bathymetry with ~ 20° and high resolution seafloor mapping that showed slope angles up to 35° (Vanneste et al., 2006). Even though the shelf-break slope angles were likely underestimated in the model, shelf-break slope angles in the north of HT are still considerably higher with 10° compared to 4° off IT

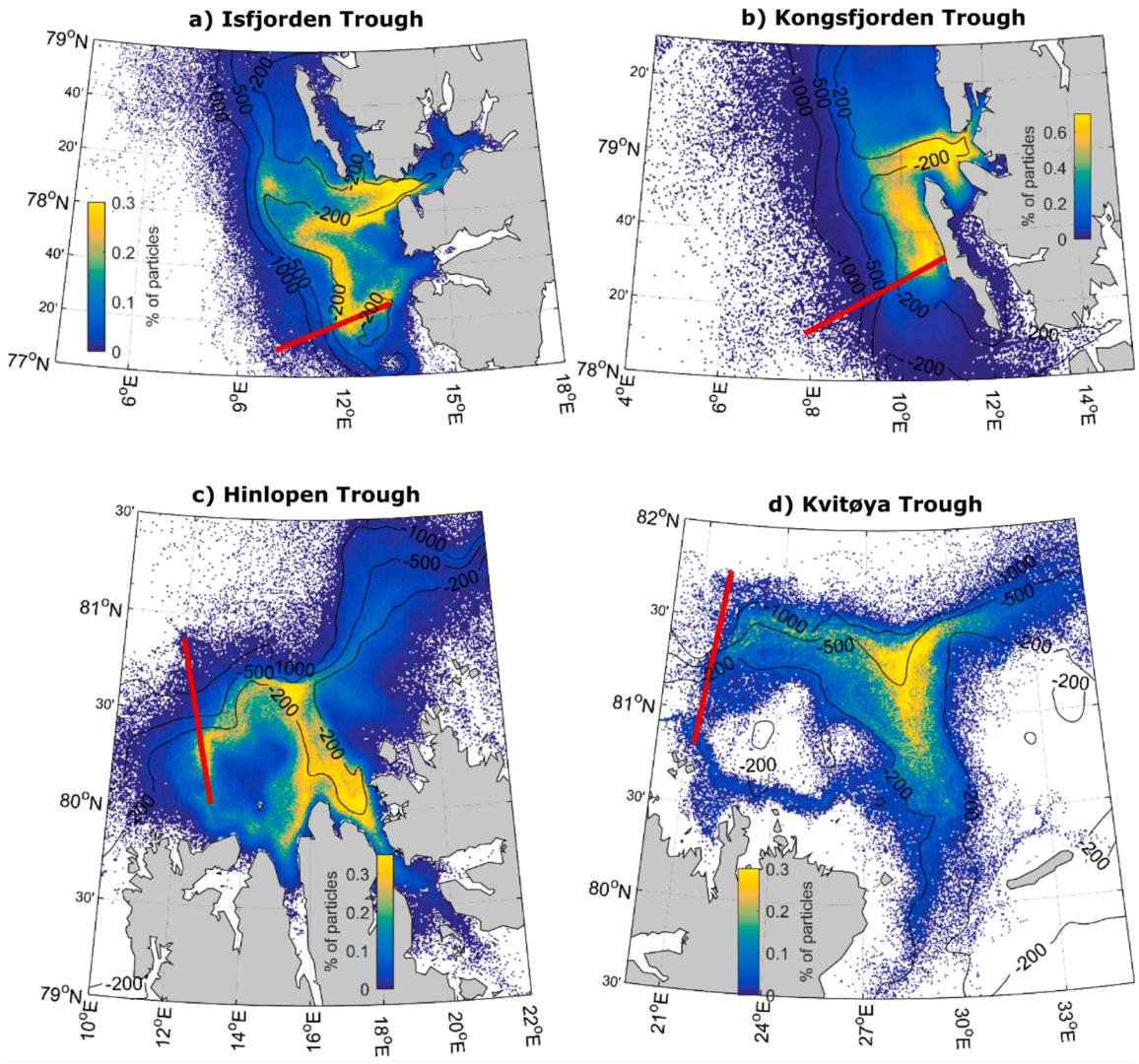

Fig. 7. Distribution of trajectories that are seeded along the red upstream transect and enter the trough. Color indicates the percentage of trajectories (particles) that pass through each model grid cell. Each panel has a different color scale. The black lines show the 1000, 500 and 200 m isobath. (For interpretation of the references to color in this figure legend, the reader is referred to the web version of this article.)

and KT, and 7° off KviT. To conserve potential vorticity, a steeper slope angle results in a narrower and faster boundary current (Cushman-Roisin and Beckers, 2011). The steep and irregular bathymetry, and corresponding vorticity imbalance, encountered by the AW boundary current, likely leads to the generation of eddies and meanders. This has been observed in the S800 model with eddy detecting algorithms; Crews et al. (2018) found frequent formation of eddies in front of the HT which stayed trapped within Sofia Deep until dissolution.

At HT, the AW boundary current encounters both a steeper shelf-break, and a deeper and steeper trough opening than at IT, KT and KviT. The HT is between 50 and 100 m deeper than IT and KviT and is characterized by its regular shape in form of a ~350 m deep and ~120 km long trench. This difference also becomes apparent in the maps in Figs. 3 and 4: HT is the only trough where the 300 m isobath reaches from trough opening to end. The combination of the deep trough opening, the steep shelf-break and the steep trough slope can explain the increased topographic steering of AW into the HT.

The average circulation in KviT showed a more complex recirculation pattern with contributions from both the AW boundary current and the shelf waters east of the trough (Fig. 4). Compared to the other three troughs, KviT has a ~300 m deep rise at its opening that partly shields the 400 m deep trough from AW inflow. On the southern side of this rise, shelf water is flowing into the trough and flows southward as a strong boundary current, together with AW entering the trough along the western trough slope (between the 100 and 200 m isobath). The sill area likely experiences very dynamic circulation patterns since the eastward flowing AW interfaces the westward flowing shelf water. This circulation pattern differs slightly from a recent ADCP survey which only found AW inflow into the trough (Pérez-Hernández et al., 2017). However, the magnitude of the AW inflow agrees (0.2 Sv) with our model and the ADCP survey was only a synoptic snapshot which is difficult to compare to the long-term average presented here. The inflow of AW into the Barents Sea through KviT has also been confirmed by current measurement and CTD profiles in the area (Aagaard et al., 1983; Lind and Ingvaldsen, 2012). The AW flowing into the Barents Sea from the north loses heat to the overlying Arctic Water and is an important driver of Barents Sea warming (Lind and Ingvaldsen, 2012).

Both IT and KT experience distinctly more seasonal (winter intensified) inflows than HT and KviT do (Fig. 6). The winter intensified flow is likely related to the seasonality of WSC volume transport; mooring observations showed that the WSC is strongest in the winter months (Beszczynska-Moller et al., 2012). The increased AW transport in winter likely enhances AW flow into the troughs due to a faster and broader WSC core along the shelf-break (Nilsen et al., 2016). Seasonally

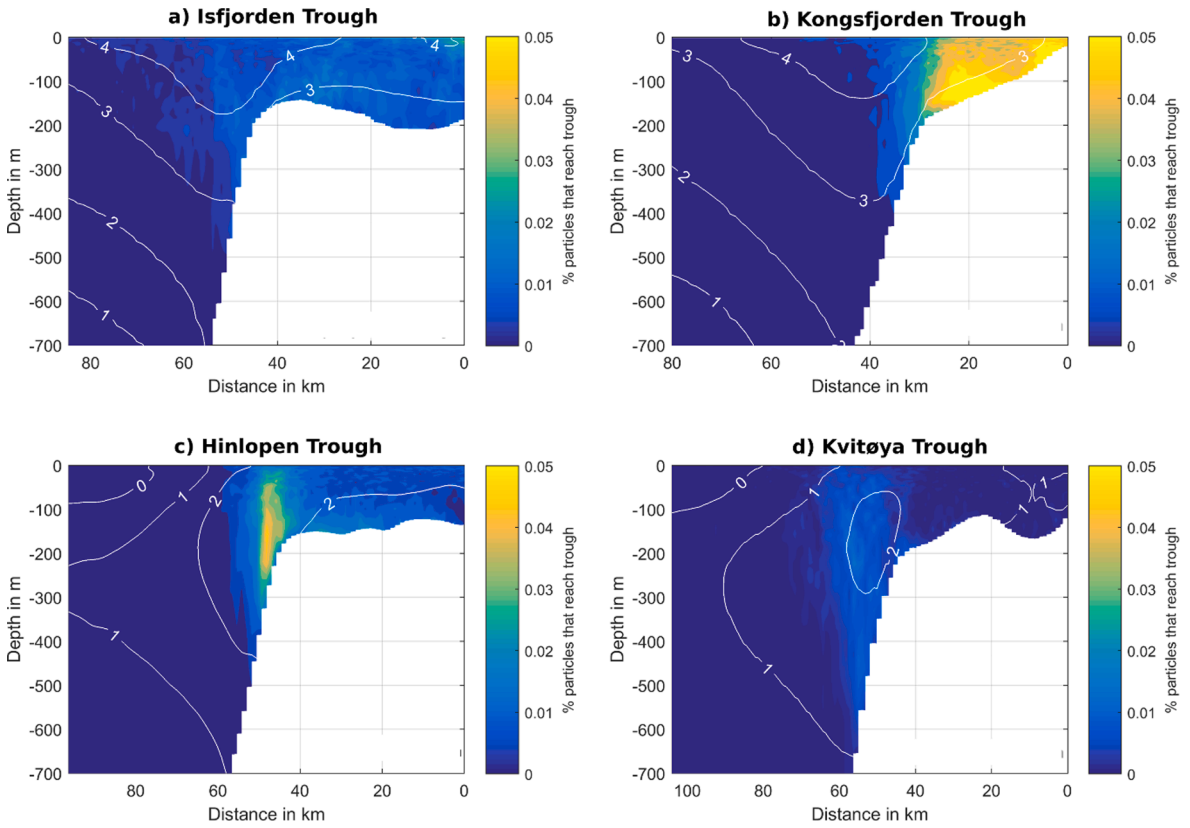

Fig. 8. Sections across the shelf-break (marked as red lines in Fig. 7) showing the start location and depth of particles that enter each trough. Color indicates the percentage of trajectories that start in each grid cell and enter the trough. White contours mark the average modelled temperature for each section in °C. (For interpretation of the references to color in this figure legend, the reader is referred to the web version of this article.)

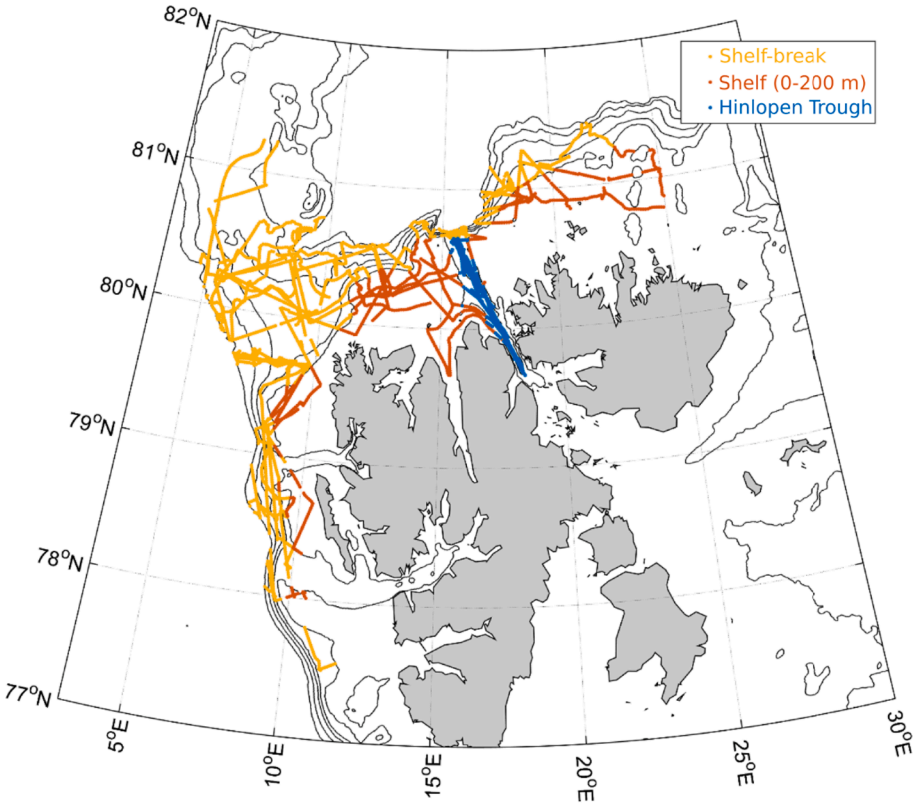

Fig. 9. Location of echosounder data used to average the profiles in Fig. 10. Bathymetry contours are shown as solid black lines in 200 m intervals up to 1000 m depth. The bathymetric data was retrieved from the International Bathymetric Chart of the Arctic Ocean (Jakobsson et al., 2012).

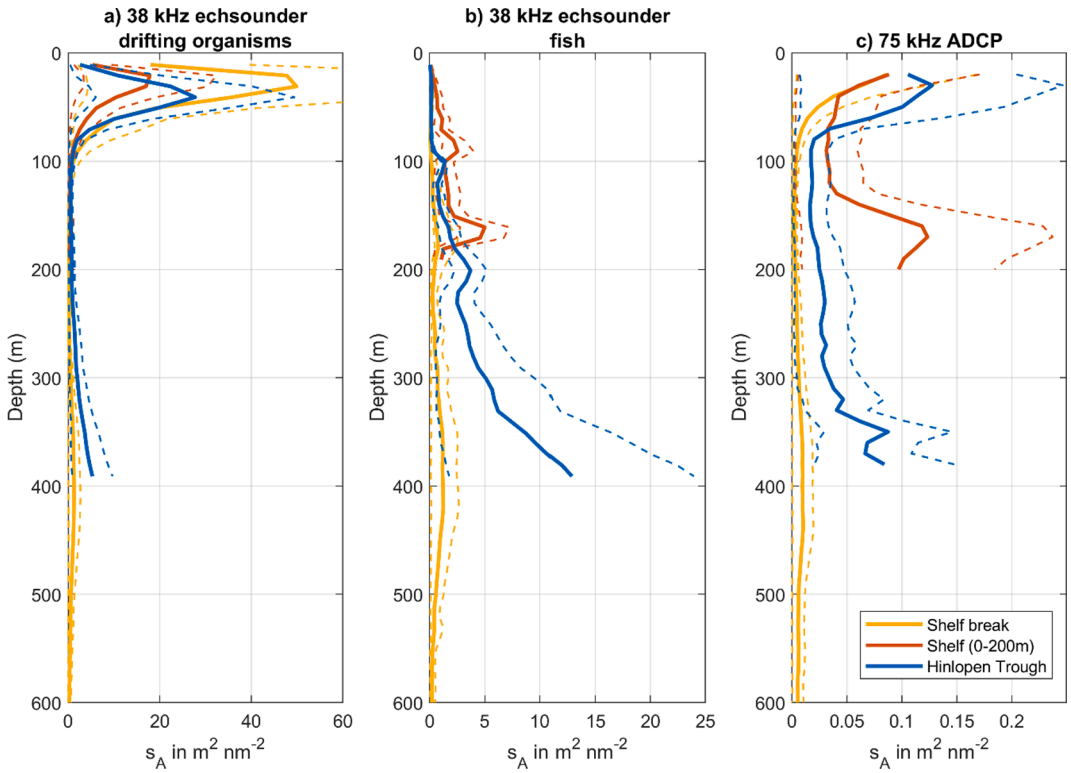

Fig. 10. Comparison of averaged acoustic backscatter profiles, between the shelf (yellow), shelf-break (red), and Hinlopen Trough (dark blue). Panel a) shows 38 kHz backscatter from drifting organisms, panel b) 38 kHz backscatter from fish and panel c) the total 75 kHz backscatter. The thick lines show the mean profiles and the dashed lines the bootstrapped 95% confidence intervals. The data was gathered between July and September 2014 to 2019. (For interpretation of the references to color in this figure legend, the reader is referred to the web version of this article.)

increased transport is also found in the AW boundary current further downstream at 30°E; mooring observations east of KviT showed increased volume transport, salinity and temperature from November to January (Pérez-Hernández et al., 2019).

The AW entering the Arctic north of Svalbard is significantly cooled along its path, losing its heat to the atmosphere, sea ice and through lateral mixing (Renner et al., 2018). This is reflected in our AW transport time series (Fig. 6), where the AW inflow into HT and KviT shows a stronger seasonal cycle than the total inflow. The seasonal cycle of the total inflow and the 1. PC (recirculation component) becomes weaker for each trough in the down-stream direction (Fig. 6). This could indicate that a part of the increased WSC transport in winter is recirculated in Fram Strait, since not only volume transport but also instability and recirculation along the Yermak Plateau increases in winter (Crews et al., 2019; Hattermann et al., 2016; von Appen et al., 2016). For KviT, the small amount of AW inflow from the shelf-break (Fig. 8) and reduced seasonality of the total inflow indicate that much of the recirculating water is derived from the shelf, as indicated in Fig. 4.

4.2. Interpretation of acoustic backscatter observations

A comparison of the 38 kHz echosounder and catch data in the area found that the surface scattering layer mainly consisted of advected young-of-the-year fish and mesozooplankton (Knutsen et al., 2017; Gjøsæter et al., 2017). The mesopelagic scattering layer consisted of zooplankton and pelagic fish of boreal and Arctic origins (Geoffroy et al., 2019). In HT the mesopelagic and demersal scattering layer comprised especially krill (*Thysanoessa* spp.) and amphipods (Knutsen et al., 2017).

The composition of fish species contributing to the acoustic backscatter varied somewhat among years and within the surveyed area (Ingvaldsen et al., 2016a, 2016b, 2017a, 2017b). Young-of-the-year fish of various species, occupying the surface layer, dominated in terms of 38 kHz backscattering strength. Of adult fish, Atlantic cod was the dominating species and they were mainly confined to near-bottom areas at the shelf and along the shelf-break down to about 700 m. Capelin, haddock, beaked redfish and polar cod ranged next in terms of fish biomass. Backscatter from fish near the sea floor was found mainly to stem from various demersal fish species like cod and haddock, while pelagic fish at mesopelagic depths mostly consisted of lanternfishes and other mesopelagic fish species (Knutsen et al., 2017). Cod were also detected at mesopelagic depths over deep water in low quantities (Ingvaldsen et al., 2017). The increased presence of fish in HT suggests a rich local zooplankton and benthos prey biomass (Ingvaldsen et al., 2016a,b).

ADCP backscatter in the region is mainly caused by krill, the copepods *Calanus* spp., the medusa *Cyanea capillata*, the amphipod *Themisto libellula*, and euphausiids such as *Meganyctiphanes norvegica* (Berge et al., 2014; Cottier et al., 2006). The organisms in the mesopelagic scattering layer in the Svalbard area show complex diel vertical migration patterns (Berge et al., 2014; Falk-Petersen et al., 2008; Gjøsæter et al., 2017), that could affect our interpretation of the spatial backscatter distribution. We compared the backscatter profiles recorded between 06:00–18:00 and 18:00–06:00 in suppl. Fig. 15 and found that the averaged profiles show only minimal differences. The differences between the shelf-break, shelf and HT remain the same during day and night and diel vertical migration does not affect our interpretation of the large-scale patterns. During night in HT, backscatter from fish was less concentrated to the demersal layer and more spread over the entire water column but still stronger than on the shelf and shelf break.

4.3. Hinlopen trough as favorable habitat

HT was the only trough sufficient covered by our backscatter dataset and showed very high levels of backscatter from fish compared to the shelf and shelf-break north of Svalbard (Fig. 10). Thus, we will focus the remaining discussion on HT and argue that HT is a special habitat where

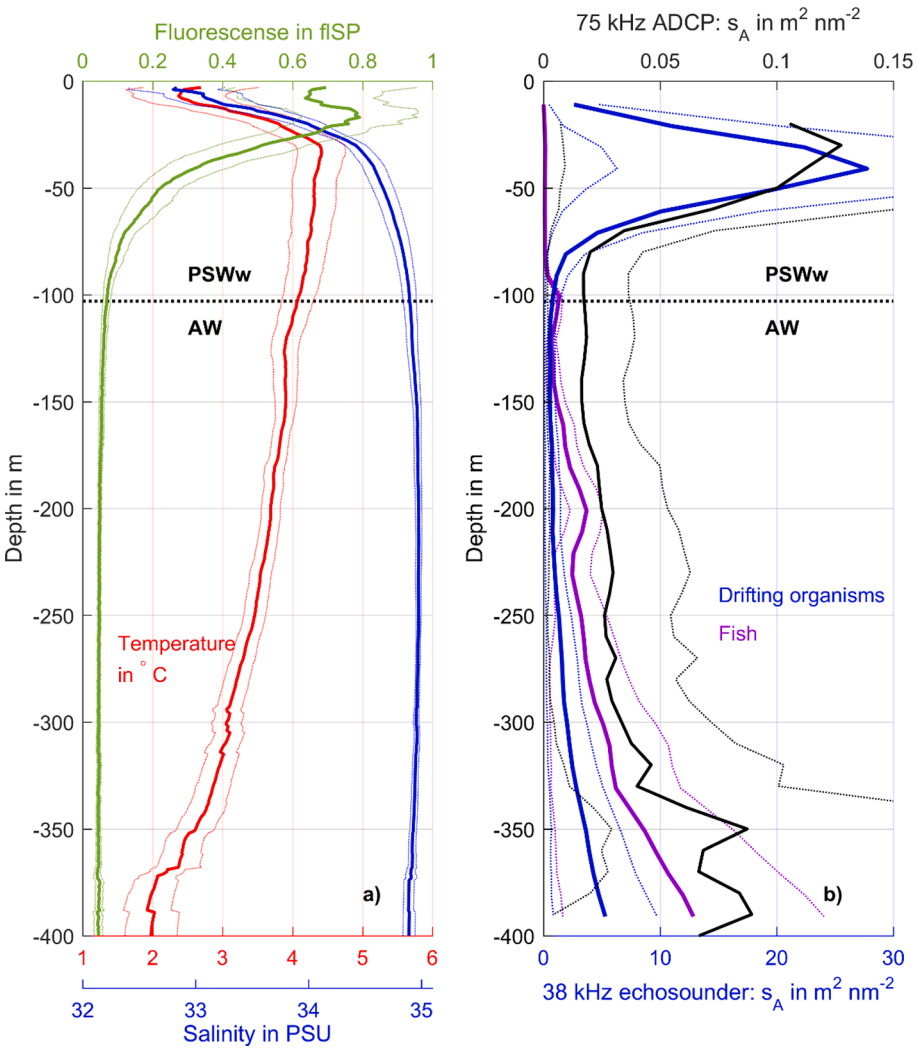

Fig. 11. Comparison between averaged temperature, salinity and fluorescence profiles in panel a) and averaged acoustic backscatter profiles in panel b). The profiles were averaged from CTD and backscatter profiles in Hinlopen Trough that cover July and September 2014 to 2019. The thick lines show the mean profiles and the dashed line the 95% confidence intervals. The black horizontal dashed line marks the border between warm Polar Surface Water (PSWw, T < 0 °C and S > 34.9 PSU) and Atlantic Water (AW, T > 0 °C and S > 34.9 PSU).

the Atlantic-advective domain is extended onto the Svalbard shelf. The modelled currents and particle tracks showed that the four troughs receive topographically steered AW inflow (Figs. 3 and 4 and 7) and particle throughflow and retention. The trough can be seen as a hybrid between the shelf-break, where the boundary current supplies a steady nutrient and biomass supply but drifting organisms are swept away rapidly, and the shelf, where drifting organisms are more stationary but there is only sporadic replenishment of the nutrient and biomass supply.

Surveys of benthic biomass north of Svalbard found rich benthic communities in the Hinlopen Strait, and suggested that this was caused by a large supply of organic matter from inflowing AW, as benthos growth in the area is primarily food limited (Carroll and Ambrose, 2012; Meyer et al., 2015). Our model results confirm a strong and steady inflow of AW into HT, and our hydrographic data confirmed this by showing the highest backscatter (below the euphotic zone) in modified AW in the trough (Figs. 10 and 11). The frequent sighting of baleen whales in the HT area (Storrie et al., 2018; Vacquié-Garcia et al., 2017), high euphausiid and calanus biomass (Ressler et al., 2015; Søreide et al., 2008) and active Northern prawn fisheries (Misund et al., 2016) in the trough mark out the HT as special habitat along the shelf.

Our comparison of average backscatter profiles showed that HT has higher levels of backscatter in the demersal and mesopelagic layer (AW layer) than the shelf-break (Fig. 10a and c) and that HT contains large aggregations of fish compared to the shelf and shelf-break north of Svalbard (Fig. 10b). The fish visible as strong 38 kHz scatterers in Fig. 10 in HT likely congregate in the trough to feed on the rich zooplankton and benthic biomass (Knutsen et al., 2017; Meyer et al., 2015). The observation that surface layer 38 kHz backscatter was larger in HT than on the shelf and shelf-break during some surveys points to enhanced primary production in the trough. The surface layer peak of backscatter in HT shown in Fig. 11 is likely related to local production in the euphotic Polar Surface Water layer fueled by upward mixing of nutrients from the nutrient-rich AW (Randelhoff et al., 2015).

We suggest three mechanisms by which the inflow and recirculation of AW can create a favorable habitat inside HT and potentially also the other troughs along the Svalbard shelf: 1) The advection of heat, nutrients and phytoplankton into the trough increases local primary and secondary production. 2) The advection of zooplankton into the trough enhances local prey availability and creates favorable feeding conditions. 3) The balance between throughflow and retention creates a favorable habitat where drifting organisms and biomass are retained longer in the trough than in a similar area on the shelf-break by the recirculating flow, yet are replenished by the AW inflow more often than in a similar area on the shelf.

5. Conclusions

We could show that the Isfjorden, Kongsfjorden, Hinlopen and Kvitøya trough receive topographically steered Atlantic Water inflow, that partially recirculates within the troughs. Of these troughs, the Hinlopen Trough receives the most direct inflow from the Atlantic Water boundary current. Acoustic Doppler current profiler and echosounder

observations showed stronger backscatter from fish in the Hinlopen Trough compared to the shelf and shelf-break north of Svalbard and higher levels of mesopelagic and demersal layer backscatter in the trough than on the shelf-break. The steep bathymetry and steady Atlantic Water inflow likely create a favorable feeding habitat in Hinlopen Trough for fish, benthic organisms and marine mammals. The troughs along the Svalbard shelf are hybrid (between the shelf and shelf-break) habitats where the Atlantic-advective domain is extended closer to the Svalbard coastline.

Declaration of Competing Interest

The authors declare that they have no known competing financial interests or personal relationships that could have appeared to influence the work reported in this paper.

Acknowledgements

We would like to thank the crew and scientists onboard *RV Helmer Hanssen*, *RV Håkon Mosby* and *RV Oceania* for collecting and sharing ADCP, CTD and echosounder data. The ocean model simulations were produced by the Fram Centre "Arctic Ocean" flagship project "Mesoscale modeling of Ice, Ocean, and Ecology of the Arctic Ocean (ModOIE, project number 66060)." ModOIE simulation fields are available at data.npolar.no (doi:10.21334/npolar.2017.2f52acd2). We thank the reviewers for their constructive feedback.

Funding

We declare no competing interests. Financial support of the study comes from The Research Council of Norway through the project "The Arctic Ocean Ecosystem" – (SI_ARCTIC, RCN 228896) and from the Institute of Marine Research, Bergen.

References

Aagaard, K., Foldvik, A., Gammelsrød, T., Vinje, T., 1983. One-year records of current and bottom pressure in the strait between Nordaustlandet and Kvitøya, Svalbard, 1980–81. Polar Res. 1, 107–113. https://doi.org/10.1111/j.1751-8369.1983.tb00695.x.

Asbjørnsen, H., Årthun, M., Skagseth, Ø., Eldevik, T., 2020. Mechanisms Underlying Recent Arctic Atlantification. Geophys. Res. Lett. 47 https://doi.org/10.1029/2020GL088036.

Basedow, S.L., Sundfjord, A., von Appen, W.-J., Halvorsen, E., Kwasniewski, S., Reigstad, M., 2018. Seasonal Variation in Transport of Zooplankton Into the Arctic Basin Through the Atlantic Gateway, Fram Strait. Front. Mar. Sci. 5, 1–22. https://doi.org/10.3389/fmars.2018.00194.

Berge, J., Cottier, F., Varpe, Ø., Renaud, P.E., Falk-Petersen, S., Kwasniewski, S., Griffiths, C., Søreide, J.E., Johnsen, G., Aubert, A., Bjærke, O., Hovinen, J., Jung-Madsen, S., Tveit, M., Majaneva, S., 2014. Arctic complexity: A case study on diel vertical migration of zooplankton. J. Plankton Res. 36, 1279–1297. https://doi.org/10.1093/plankt/fbu059.

Beszczynska-Moller, A., Fahrbach, E., Schauer, U., Hansen, E., 2012. Variability in Atlantic water temperature and transport at the entrance to the Arctic Ocean, 1997–2010. ICES J. Mar. Sci. 69, 852–863. https://doi.org/10.1093/icesjms/fss056.

Bluhm, B.A., Kosobokova, K.N., Carmack, E.C., 2015. A tale of two basins: An integrated physical and biological perspective of the deep Arctic Ocean. Prog. Oceanogr. 139, 89–121. https://doi.org/10.1016/j.pocean.2015.07.011.

Budgell, W.P., 2005. Numerical simulation of ice-ocean variability in the Barents Sea region. Ocean Dyn. 55, 370–387. https://doi.org/10.1007/s10236-005-0008-3.

Carroll, M.L., Ambrose, W.G., 2012. Benthic infaunal community variability on the northern Svalbard shelf. Polar Biol. 35, 1259–1272. https://doi.org/10.1007/s00300-012-1171-x.

Cottier, F., Tverberg, V., Inall, M., Svendsen, H., Nilsen, F., 2005. Water mass modification in an Arctic fjord through cross-shelf exchange : The seasonal hydrography of Kongsfjorden. Svalbard 110, 1–18. https://doi.org/10.1029/2004JC002757.

Cottier, F.R., Nilsen, F., Enall, M.E., Gerland, S., Tverberg, V., Svendsen, H., 2007. Wintertime warming of an Arctic shelf in response to large-scale atmospheric circulation. Geophys. Res. Lett. 34, 1–5. https://doi.org/10.1029/2007GL029948.

Cottier, F.R., Tarling, G.A., Wold, A., Falk-Petersen, S., 2006. Unsynchronized and synchronized vertical migration of zooplankton in a high arctic fjord. Limnol. Oceanogr. 51, 2586–2599. https://doi.org/10.4319/lo.2006.51.6.2586.

Crews, L., Sundfjord, A., Albretsen, J., Hattermann, T., 2018. Mesoscale Eddy Activity and Transport in the Atlantic Water Inflow Region North of Svalbard. J. Geophys. Res. Ocean. 123, 201–215. https://doi.org/10.1002/2017JC013198.

Crews, L., Sundfjord, A., Hattermann, T., 2019. How the Yermak Pass Branch Regulates Atlantic Water Inflow to the Arctic Ocean. J. Geophys. Res. Ocean. 124, 267–280. https://doi.org/10.1029/2018JC014476.

Cushman-Roisin, B., Beckers, J.M., 2011. Introduction to Geophysical Fluid Dynamics: Physical and Numerical Aspects. International Geophysics. Elsevier Science.

Deines, K.L., 1999. Backscatter estimation using Broadband acoustic Doppler current profilers, in: Proceedings of the IEEE Sixth Working Conference on Current Measurement (Cat. No.99CH36331). IEEE, pp. 249–253. https://doi.org/10.1109/CCM.1999.755249.

Döös, K., 1995. Interocean exchange of water masses. J. Geophys. Res. Ocean. 100, 13499–13514. https://doi.org/10.1029/95JC00337.

Falk-Petersen, S., Leu, E., Berge, J., Kwasniewski, S., Nygård, H., Røstad, A., Keskinen, E., Thormar, J., von Quillfeldt, C., Wold, A., Gulliksen, B., 2008. Vertical migration in high Arctic waters during autumn 2004. Deep. Res. Part II Top. Stud. Oceanogr. 55, 2275–2284. https://doi.org/10.1016/j.dsr2.2008.05.010.

Fielding, S., Griffiths, G., Roe, H.S.J., 2004. The biological validation of ADCP acoustic backscatter through direct comparison with net samples and model predictions based on acoustic-scattering models. ICES J. Mar. Sci. 61, 184–200. https://doi.org/10.1016/j.icesjms.2003.10.011.

Fossheim, M., Primicerio, R., Johannesen, E., Ingvaldsen, R.B., Aschan, M.M., Dolgov, A. V., 2015. Recent warming leads to a rapid borealization of fish communities in the Arctic. Nat. Clim. Chang. 5, 673–677. https://doi.org/10.1038/nclimate2647.

Geissler, W.H., Gebhardt, A.C., Gross, F., Wollenburg, J., Jensen, L., Schmidt-Aursch, M. C., Krastel, S., Elger, J., Osti, G., 2016. Arctic megaslide at presumed rest. Sci. Rep. 6 https://doi.org/10.1038/srep38529.

Geoffroy, M., Daase, M., Cusa, M., Darnis, G., Graeve, M., Santana Hernández, N., Berge, J., Renaud, P.E., Cottier, F., Falk-Petersen, S., 2019. Mesopelagic Sound Scattering Layers of the High Arctic: Seasonal Variations in Biomass, Species Assemblage, and Trophic Relationships. Front. Mar. Sci. 6 https://doi.org/10.3389/fmars.2019.00364.

Gjøsæter, H., Wiebe, P.H., Knutsen, T., Ingvaldsen, R.B., 2017. Evidence of Diel Vertical Migration of Mesopelagic Sound-Scattering Organisms in the Arctic. Front. Mar. Sci. 4, 1–14. https://doi.org/10.3389/fmars.2017.00332.

Gostiaux, L., van Haren, H., 2010. Extracting meaningful information from uncalibrated backscattered echo intensity data. J. Atmos. Ocean. Technol. 27, 943–949. https://doi.org/10.1175/2009JTECHO704.1.

Goszczko, I., Ingvaldsen, R.B., Onarheim, I.H., 2018. Wind-Driven Cross-Shelf Exchange-West Spitsbergen Current as a Source of Heat and Salt for the Adjacent Shelf in Arctic Winters. J. Geophys. Res. Ocean. 123, 2668–2696. https://doi.org/10.1002/2017JC013553.

Haidvogel, D.B., Arango, H., Budgell, W.P., Cornuelle, B.D., Curchitser, E., Di Lorenzo, E., Fennel, K., Geyer, W.R., Hermann, A.J., Lanerolle, L., Levin, J., McWilliams, J.C., Miller, A.J., Moore, A.M., Powell, T.M., Shchepetkin, A.F., Sherwood, C.R., Signell, R.P., Warner, J.C., Wilkin, J., 2008. Ocean forecasting in terrain-following coordinates: Formulation and skill assessment of the Regional Ocean Modeling System. J. Comput. Phys. 227, 3595–3624. https://doi.org/10.1016/j.jcp.2007.06.016.

Hattermann, T., Isachsen, P.E., von Appen, W.-J., Albretsen, J., Sundfjord, A., 2016. Eddy-driven recirculation of Atlantic Water in Fram Strait. Geophys. Res. Lett. 43 https://doi.org/10.1002/2016GL068323.

Haug, T., Bogstad, B., Chierici, M., Gjøsæter, H., Hallfredsson, E.H., Høines, Å.S., Hoel, A. H., Ingvaldsen, R.B., Jørgensen, L.L., Knutsen, T., Loeng, H., Naustvoll, L.J., Røttingen, I., Sunnanå, K., 2017. Future harvest of living resources in the Arctic Ocean north of the Nordic and Barents Seas: A review of possibilities and constraints. Fish. Res. 188, 38–57. https://doi.org/10.1016/j.fishres.2016.12.002.

Inall, M.E., Nilsen, F., Cottier, F.R., Daae, R., 2015. Shelf/fjord exchange driven by coastal-trapped waves in the Arctic. J. Geophys. Res. Ocean. 120, 8283–8303. https://doi.org/10.1002/2015JC011277.

Ingvaldsen, R. B., Bucklin, A., Chierici, M., Gjøsæter, H., Haug, T., Hosia, A., Jørgensen, L.L. et al., 2016a. Cruise report SI_ARCTIC/Arctic Ecosystem survey R/V Helmer Hanssen, 17 August-7 September 2015. Toktrapport/Havforskningsinstituttet.

Ingvaldsen, R.B., Bucklin, A., Chierici, M., Gjøsæter, H., Haug, T., Hosia, A., Jørgensen, L. L., Knutsen, T., Naustvoll, L.J., Ona, E., P., W., 2016b. Cruise report SI_ARCTIC / Arctic Ecosystem survey R / V Helmer Hanssen, 17 August-7 September 2015. Toktrapport/Havforskningsinstituttet.

Ingvaldsen, R.B., Gjøsæter, H., Hallfredsson, E., Haug, T., Hosia, A., Jørgensen, L.L., Knutsen, T., et al., 2017a. Cruise report SI_ARCTIC/Arctic Ecosystem Survey R/V Helmer Hanssen, 2-16 September 2016. Toktrapport/Havforskningsinstituttet.

Ingvaldsen, R.B., Gjøsæter, H., Haug, T., Jørgensen, L.L., Knutsen, T., Lødemel, H.H., Menze, S., et al., 2017b. Cruise report SI_ARCTIC/Arctic Ecosystem Survey R/V Helmer Hanssen, 21 August-7 September 2017. Toktrapport/Havforskningsinstituttet.

Jakobsson, M., Mayer, L., Coakley, B., Dowdeswell, J.A., Forbes, S., Fridman, B., Hodnesdal, H., Noormets, R., Pedersen, R., Rebesco, M., Schenke, H.W., Zarayskaya, Y., Accettella, D., Armstrong, A., Anderson, R.M., Bienhoff, P., Camerlenghi, A., Church, I., Edwards, M., Gardner, J.V., Hall, J.K., Hell, B., Hestvik, O., Kristoffersen, Y., Marcussen, C., Mohammad, R., Mosher, D., Nghiem, S. V., Pedrosa, M.T., Travaglini, P.G., Weatherall, P., 2012. The International Bathymetric Chart of the Arctic Ocean (IBCAO) Version 3.0. Geophys. Res. Lett. 39, 1–6. https://doi.org/10.1029/2012GL052219.

Knutsen, T., Wiebe, P.H., Gjøsæter, H., Ingvaldsen, R.B., Lien, G., 2017. High Latitude Epipelagic and Mesopelagic Scattering Layers—A Reference for Future Arctic Ecosystem Change. Front. Mar. Sci. 4 https://doi.org/10.3389/fmars.2017.00334.

Koenig, Z., Provost, C., Villacieros-Robineau, N., Sennéchael, N., Meyer, A., Lellouche, J. M., Garric, G., 2017. Atlantic waters inflow north of Svalbard: Insights from IAOOS observations and Mercator Ocean global operational system during N-ICE2015. J. Geophys. Res. Ocean. 122, 1254–1273. https://doi.org/10.1002/2016JC012424.

Korneliussen, R.J., Heggelund, Y., Macaulay, G.J., Patel, D., Johnsen, E., Eliassen, I.K., 2016. Acoustic identification of marine species using a feature library. Methods Oceanogr. 17, 187–205. https://doi.org/10.1016/j.mio.2016.09.002.

Korneliussen, R.J., Ona, E., Eliassen, I., Heggelund, Y., Patel, R., Godø, O.R., 2006. The large scale survey system – LSSS. Proc. ofthe 29th Scand. Symp. Phys. Acoust.

Lind, S., Ingvaldsen, R.B., 2012. Variability and impacts of Atlantic Water entering the Barents Sea from the north. Deep. Res. Part I Oceanogr. Res. Pap. 62, 70–88. https://doi.org/10.1016/j.dsr.2011.12.007.

Lind, S., Ingvaldsen, R.B., Furevik, T., 2018. Arctic warming hotspot in the northern Barents Sea linked to declining sea-ice import. Nat. Clim. Chang. 8, 634–639. https://doi.org/10.1038/s41558-018-0205-y.

MacLennan, D.N., Fernandes, P.G., Dalen, J., 2002. A consistent approach to definitions and symbols in fisheries acoustics. ICES J. Mar. Sci. 59, 365–369. https://doi.org/10.1006/jmsc.2001.1158.

Meeren, G.I. Van Der, Prozorkevich, D., 2019. Survey report from the joint Norwegian/Russian ecosystem survey in the Barents Sea and adjacent waters, August-October 2018.

Menze, S., Ingvaldsen, R.B., Haugan, P., Fer, I., Sundfjord, A., Beszczynska-Moeller, A., Falk-Petersen, S., 2019. Atlantic Water Pathways Along the North-Western Svalbard Shelf Mapped Using Vessel-Mounted Current Profilers. J. Geophys. Res. Ocean. 124, 1699–1716. https://doi.org/10.1029/2018JC014299.

Meyer, K.S., Sweetman, A.K., Young, C.M., Renaud, P.E., 2015. Environmental factors structuring Arctic megabenthos - a case study from a shelf and two fjords. Front. Mar. Sci. 2, 1–14. https://doi.org/10.3389/fmars.2015.00022.

Misund, O.A., Heggland, K., Skogseth, R., Falck, E., Gjøsæter, H., Sundet, J., Watne, J., Lønne, O.J., 2016. Norwegian fisheries in the Svalbard zone since 1980. Regulations, profitability and warming waters affect landings. Polar Sci. 10, 312–322. https://doi.org/10.1016/j.polar.2016.02.001.

Nilsen, F., Cottier, F., Skogseth, R., Mattsson, S., 2008. Fjord-shelf exchanges controlled by ice and brine production: The interannual variation of Atlantic Water in Isfjorden. Svalbard. Cont. Shelf Res. 28, 1838–1853. https://doi.org/10.1016/j.csr.2008.04.015.

Nilsen, F., Skogseth, R., Vaardal-Lunde, J., Inall, M., 2016. A Simple Shelf Circulation Model: Intrusion of Atlantic Water on the West Spitsbergen Shelf. J. Phys. Oceanogr. 46, 1209–1230. https://doi.org/10.1175/JPO-D-15-0058.1.

Pérez-Hernández, M.D., Pickart, R.S., Pavlov, V., Våge, K., Ingvaldsen, R., Sundfjord, A., Renner, A.H.H., Torres, D.J., Erofeeva, S.Y., 2017. The Atlantic Water boundary current north of Svalbard in late summer. J. Geophys. Res. Ocean. 122, 2269–2290. https://doi.org/10.1002/2016JC012486.

Pérez-Hernández, M.D., Pickart, R.S., Torres, D.J., Bahr, F., Sundfjord, A., Ingvaldsen, R., Renner, A.H.H., Beszczynska-Möller, A., von Appen, W.-J., Pavlov, V., 2019. Structure, transport and seasonality of the Atlantic Water Boundary Current north of Svalbard: Results from a year-long mooring array. J. Geophys. Res. Ocean. 1–20 https://doi.org/10.1029/2018JC014759.

Polyakov, I.V., Pnyushkov, A.V., Alkire, M.B., Ashik, I.M., Baumann, T.M., Carmack, E. C., Goszczko, I., Guthrie, J., Ivanov, V.V., Kanzow, T., Krishfield, R., Kwok, R., Sundfjord, A., Morison, J., Rember, R., Yulin, A., 2017. Greater role for Atlantic inflows on sea-ice loss in the Eurasian Basin of the Arctic Ocean. Science 356 (6335), 285–291. https://doi.org/10.1126/science.aai8204.

Randelhoff, A., Reigstad, M., Chierici, M., Sundfjord, A., Ivanov, V., Cape, M.R., Vernet, M., Tremblay, J.-É., Bratbak, G., Kristiansen, S., 2018. Seasonality of the Physical and Biogeochemical Hydrography in the Inflow to the Arctic Ocean through Fram Strait. Front. Mar. Sci. 5, 224. https://doi.org/10.3389/fmars.2018.00224.

Randelhoff, A., Sundfjord, A., Reigstad, M., 2015. Seasonal variability and fluxes of nitrate in the surface waters over the Arctic shelf slope. Geophys. Res. Lett. 3442–3449. https://doi.org/10.1002/2015GL063655.

Renner, A.H.H., Sundfjord, A., Janout, M.A., Ingvaldsen, R.B., Beszczynska-Möller, A., Pickart, R.S., Pérez-Hernández, M.D., 2018. Variability and redistribution of heat in the Atlantic Water boundary current north of Svalbard. J. Geophys. Res. Ocean. https://doi.org/10.1029/2018JC013814.

Ressler, P.H., Dalpadado, P., Macaulay, G.J., Handegard, N., Skern-Mauritzen, M., 2015. Acoustic surveys of euphausiids and models of baleen whale distribution in the Barents Sea. Mar. Ecol. Prog. Ser. 527, 13–29. https://doi.org/10.3354/meps11257.

Rudels, B., Björk, G., Nilsson, J., Winsor, P., Lake, I., Nohr, C., 2005. The interaction between waters from the Arctic Ocean and the Nordic Seas north of Fram Strait and along the East Greenland Current: Results from the Arctic Ocean-02 Oden expedition. J. Mar. Syst. 55, 1–30. https://doi.org/10.1016/j.jmarsys.2004.06.008.

Saloranta, T.M., Svendsen, H., 2001. Across the Arctic front west of Spitsbergen: High-resolution CTD sections from 1998–2000. Polar Res. 20, 177–184. https://doi.org/10.3402/polar.v20i2.6515.

Shchepetkin, A.F., McWilliams, J.C., 2005. The regional oceanic modeling system (ROMS): A split-explicit, free-surface, topography-following-coordinate oceanic model. Ocean Model. 9, 347–404. https://doi.org/10.1016/j.ocemod.2004.08.002.

Silyakova, A., Jansson, P., Serov, P., Ferré, B., Pavlov, A.K., Hattermann, T., Graves, C.A., Platt, S.M., Myhre, C.L., Gründger, F., Niemann, H., 2020. Physical controls of dynamics of methane venting from a shallow seep area west of Svalbard. Cont. Shelf Res. 194, 104030 https://doi.org/10.1016/j.csr.2019.104030.

Skagseth, Ø., Furevik, T., Ingvaldsen, R., Loeng, H., Mork, K.A., Orvik, K.A., Ozhigin, V., 2008. Volume and heat transports to the Arctic Ocean via the Norwegian and Barents seas. Arctic-Subarctic Ocean Fluxes Defin. Role North. Seas Clim. https://doi.org/10.1007/978-1-4020-6774-7_3.

Smedsrud, L.H., Esau, I., Ingvaldsen, R.B., Eldevik, T., Haugan, P.M., Li, C., Lien, V.S., Olsen, A., Omar, A.M., Risebrobakken, B., Sandø, A.B., Semenov, V.A., Sorokina, S. A., 2013. The role of the Barents Sea in the Arctic climate system. Rev. Geophys. 51, 415–449. https://doi.org/10.1002/rog.20017.

Søreide, J.E., Falk-Petersen, S., Hegseth, E.N., Hop, H., Carroll, M.L., Hobson, K.A., Blachowiak-Samolyk, K., 2008. Seasonal feeding strategies of *Calanus* in the high-Arctic Svalbard region. Deep. Res. Part II Top. Stud. Oceanogr. 55, 2225–2244. https://doi.org/10.1016/j.dsr2.2008.05.024.

Spreen, G., Kaleschke, L., Heygster, G., 2008. Sea ice remote sensing using AMSR-E 89-GHz channels. J. Geophys. Res. 113, C02S03. https://doi.org/10.1029/2005JC003384.

Storrie, L., Lydersen, C., Andersen, M., Wynn, R.B., Kovacs, K.M., 2018. Determining the species assemblage and habitat use of cetaceans in the Svalbard Archipelago, based on observations from 2002 to 2014. Polar Res. 37, 1463065. https://doi.org/10.1080/17518369.2018.1463065.

Tverberg, V., Nost, O.A., 2009. Eddy overturning across a shelf edge front: Kongsfjorden, west Spitsbergen. J. Geophys. Res. Ocean. 114 https://doi.org/10.1029/2008JC005106.

Vacquié-Garcia, J., Lydersen, C., Marques, T.A., Aars, J., Ahonen, H., Skern-mauritzen, M., Øien, N., Kovacs, K.M., 2017. Late summer distribution and abundance of ice-associated whales in the Norwegian High Arctic. https://doi.org/10.3354/esr00791.

Vanneste, M., Harbitz, C.B., Blasio, F.V. De, Glimsdal, S., Mienert, J., Elverhøi, A., 2010. The Hinlopen-Yermak landslide, Arctic Ocean. Geomorphology, landslide dynamics and tsunami simulations. Mass-Transport Depos. Deep. Settings 95, 1–19. https://doi.org/10.2110/sepmsp.096.509.

Vanneste, M., Mienert, J., Buenz, S., 2006. The Hinlopen Slide: A giant, submarine slope failure on the northern Svalbard margin. Arctic Ocean. Earth Planet. Sci. Lett. 245, 373–388. https://doi.org/10.1016/j.epsl.2006.02.045.

Vernet, M., Ellingsen, I.H., Seuthe, L., Slagstad, D., Cape, M.R., Matrai, P.A., 2019. Influence of Phytoplankton Advection on the Productivity Along the Atlantic Water Inflow to the Arctic Ocean. Front. Mar. Sci. 6, 1–18. https://doi.org/10.3389/fmars.2019.00583.

von Appen, W.-J., Schauer, U., Hattermann, T., Beszczynska-Möller, A., 2016. Seasonal cycle of mesoscale instability of the West Spitsbergen Current. J. Phys. Oceanogr. https://doi.org/10.1175/JPO-D-15-0184.1. JPO-D-15-0184.1.

Wassmann, P., Kosobokova, K.N., Slagstad, D., Drinkwater, K.F., Hopcroft, R.R., Moore, S.E., Ellingsen, I., Nelson, R.J., Carmack, E., Popova, E., Berge, J., 2015. The contiguous domains of Arctic Ocean advection: Trails of life and death. Prog. Oceanogr. 139, 42–65. https://doi.org/10.1016/j.pocean.2015.06.011.

Wassmann, P., Slagstad, D., Ellingsen, I., 2019. Advection of Mesozooplankton Into the Northern Svalbard Shelf Region. Front. Mar. Sci. 6, 1–10. https://doi.org/10.3389/fmars.2019.00458.

Wekerle, C., Wang, Q., von Appen, W.-J., Danilov, S., Schourup-Kristensen, V., Jung, T., 2017. Eddy-Resolving Simulation of the Atlantic Water Circulation in the Fram Strait With Focus on the Seasonal Cycle. J. Geophys. Res. Ocean. 122, 8385–8405. https://doi.org/10.1002/2017JC012974.

Węsławski, J.M., Hacquebord, L., Stempniewicz, L., Malinga, M., 2000. Greenland whales and walruses in the Svalbard food web before and after exploitation. Oceanologia 42, 37–56.

Winkelmann, D., Geissler, W., Schneider, J., Stein, R., 2008. Dynamics and timing of the Hinlopen/Yermak Megaslide north of Spitsbergen, Arctic Ocean. Mar. Geol. 250, 34–50. https://doi.org/10.1016/j.margeo.2007.11.013.